ADVANCED MATERIALS
www.advmat.de

Reliable Piezoelectricity in Bilayer WSe_2 for Piezoelectric Nanogenerators

Ju-Hyuck Lee, Jae Young Park, Eun Bi Cho, Tae Yun Kim, Sang A. Han, Tae-Ho Kim, Yanan Liu, Sung Kyun Kim, Chang Jae Roh, Hong-Joon Yoon, Hanjun Ryu, Wanchul Seung, Jong Seok Lee, Jaichan Lee, and Sang-Woo Kim**

Recently, piezoelectricity has been observed in 2D atomically thin materials, such as hexagonal-boron nitride, graphene, and transition metal dichalcogenides (TMDs). Specifically, exfoliated monolayer MoS_2 exhibits a high piezoelectricity that is comparable to that of traditional piezoelectric materials. However, monolayer TMD materials are not regarded as suitable for actual piezoelectric devices due to their insufficient mechanical durability for sustained operation while Bernal-stacked bilayer TMD materials lose noncentrosymmetry and consequently piezoelectricity. Here, it is shown that WSe_2 bilayers fabricated via turbostratic stacking have reliable piezoelectric properties that cannot be obtained from a mechanically exfoliated WSe_2 bilayer with Bernal stacking. Turbostratic stacking refers to the transfer of each chemical vapor deposition (CVD)-grown WSe_2 monolayer to allow for an increase in degrees of freedom in the bilayer symmetry, leading to noncentrosymmetry in the bilayers. In contrast, CVD-grown WSe_2 bilayers exhibit very weak piezoelectricity because of the energetics and crystallographic orientation. The flexible piezoelectric WSe_2 bilayers exhibit a prominent mechanical durability of up to 0.95% of strain as well as reliable energy harvesting performance, which is adequate to drive a small liquid crystal display without external energy sources, in contrast to monolayer WSe_2 for which the device performance becomes degraded above a strain of 0.63%.

Recent studies on atomic layered materials, such as hexagonal-boron nitride (h-BN), graphene, and transition-metal dichalcogenide (TMD) materials, have reported on the piezoresponse of these materials as an external force is applied due to their broken inversion symmetry.[1–10] TMD materials exhibit a strong piezoelectricity in their monolayer configuration, but the piezoelectric effect disappears or is significantly reduced when more than two layers are present.[1,2,6] Piezoelectric devices employing monolayer TMD materials are not practically feasible because they lack the mechanical durability that is needed, and such mechanical robustness is crucial to develop useful piezoelectric devices that can be engineered using a multilayered structure.[11,12] However, multilayered TMDs have a greatly reduced or absent piezoelectricity since the continuous growth of multilayered TMD leads to a stable stacking structure with alternating polarization directions in neighboring layers. On the other hand, the polarization can be manipulated via layer-by-layer stacking (called turbostratic stacking) to induce or enhance the degree of noncentrosymmetry.[1,2,6] Here, we report on a simulation and experimental observation of piezoelectricity in mono/bilayer tungsten diselenide (WSe_2) synthesized via chemical vapor deposition (CVD) and turbostratic stacking. The piezoelectricity and mechanical durability of the mono/bilayer WSe_2 were assessed by conducting piezoresponse force microscopy (PFM) measurements, a density functional theory (DFT) simulation, and fabricating and characterizing the piezoelectric energy harvesters (PEHs). Large-area WSe_2 monolayers were grown via CVD, followed by transferring the monolayers in sequence onto a flexible polyethylene terephthalate (PET) substrate. This stacking provides the bilayers with an increase in degrees of freedom for the noncentrosymmetry. The WSe_2 bilayers with turbostratic stacking exhibit strong piezoelectricity and outstanding mechanical durability over a wide range of strain and are also capable of harvesting enough energy to operate a small liquid crystal display (LCD) without applying any external bias.

Figure 1a shows a schematic illustration of the PEH with monolayer WSe_2 (m-WSe_2) and a Cr/Au electrode on a PET substrate. In our experiment, m-WSe_2 with a grain size of 30–50 μm was synthesized using CVD on a sapphire substrate and was then transferred onto the flexible PET substrate using

Dr. J.-H. Lee, T. Y. Kim, Dr. S. A. Han, Y. Liu, Prof. S.-W. Kim
SKKU Advanced Institute of Nanotechnology (SAINT)
Sungkyunkwan University (SKKU)
Suwon 440-746, Republic of Korea
E-mail: kimsw1@skku.edu
J. Y. Park, E. B. Cho, T.-H. Kim, S. K. Kim, H.-J. Yoon, H. Ryu, W. Seung, Prof. J. Lee, Prof. S.-W. Kim
School of Advanced Materials Science and Engineering
Sungkyunkwan University (SKKU)
Suwon 440-746, Republic of Korea
E-mail: jclee@skku.edu
C. J. Roh, Prof. J. S. Lee
Department of Physics and Photon Science
Gwangju Institute of Science and Technology (GIST)
Gwangju 61005, Republic of Korea
The ORCID identification number(s) for the author(s) of this article can be found under https://doi.org/10.1002/adma.201606667.

DOI: 10.1002/adma.201606667

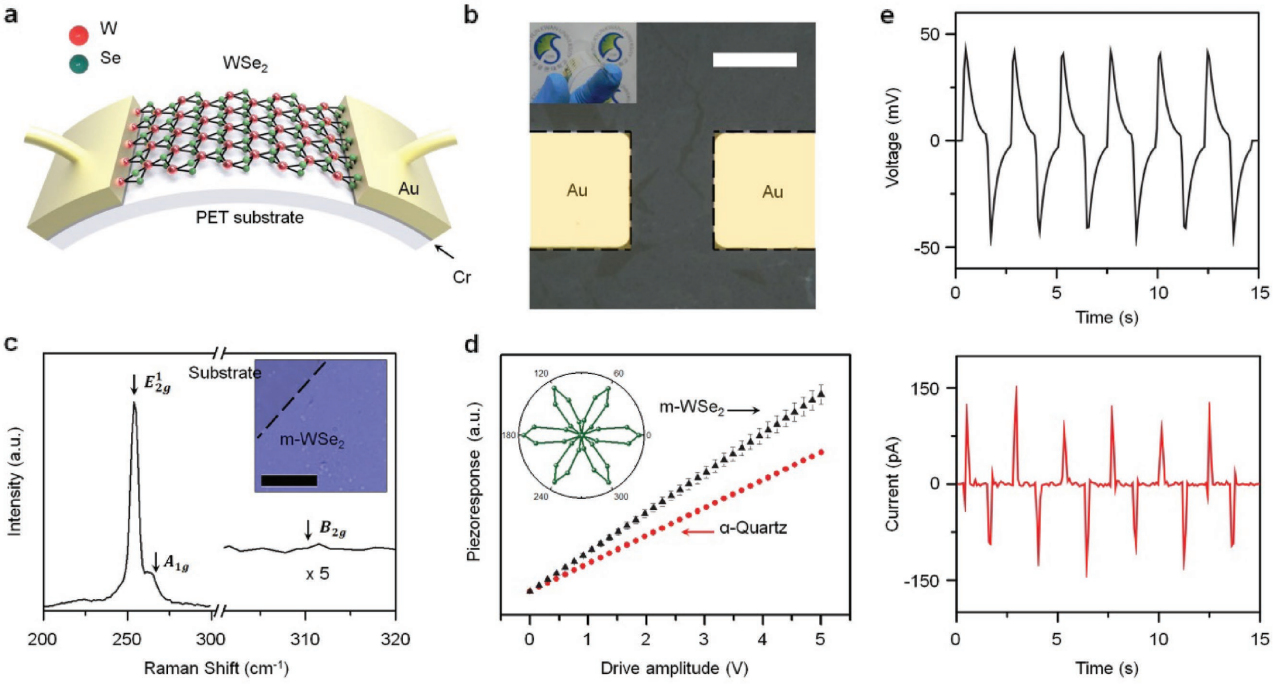

Figure 1. a) Schematic of the PEH based on monolayer WSe_2. The PEHs consisted of W, Se, Cr/Au electrode and PET substrate. The red and green spheres represent the W and Se atoms, respectively. b) Optical image of the electrode configuration. Width: 100 µm, length: 50 µm, scale bar: 50 µm. Inset: photo image of the WSe_2-based flexible piezoelectric device. c) Raman spectrum of monolayer WSe_2. Inset: optical microscopy image showing the formation of large-area monolayer WSe_2. Scale bar: 20 µm. d) Lateral piezoresponse of monolayer WSe_2 and α-Quartz using lateral PFM methods. The measured piezoelectric coefficient of monolayer WSe_2 is 3.26 ± 0.3 pm V^{-1} (black triangle), which is a higher value than that of α-quartz 2.3 pm V^{-1} (red circle). e) Output voltage response with 1 GΩ external load (top), and output short circuit current response (down) of monolayer WSe_2 under periodic tensile strain.

a simple wet transfer method (Figures S1 and S2 and Note S1, Supporting Information).[13–15] To investigate the piezoresponse of the m-WSe_2, two electrodes made of Cr/Au (5/50 nm) were deposited onto the transferred m-WSe_2 with a 100 µm width and a 50 µm length. Figure 1b presents an optical microscope image of the electrode configurations and a photo image of the fabricated PEH (inset). The number of layers was confirmed via Raman spectroscopy for the large area WSe_2 (Figure 1c, and Figure S3 and Note S2, Supporting Information).[13,16,17] The piezoelectricity in the m-WSe_2 devices is predicted by a six-fold pattern obtained from second harmonic generation (SHG) measurements, reflecting the threefold rotational symmetry of the crystal (Inset of Figure 1d and Figure S4, and Note S3, Supporting Information).[18–22] To observe the direct piezoelectricity in the m-WSe_2, the lateral piezoresponse of the m-WSe_2 was measured via PFM (Figure 1d, Figure S5 and Note S4, Supporting Information).[23] The piezoelectric coefficient d_{11} of the m-WSe_2 was estimated to be 3.26 ± 0.3 pm V^{-1}, which is reasonable value compare to previously reported simulation result (2.79 pm V^{-1}).[3] α-quartz was characterized for a comparison and exhibited d_{11} of 2.3 pm V^{-1}, which is close to earlier reported value.[24] The m-WSe_2 was also characterized in terms of their piezoelectric output voltage and current response (Figure 1e, Figures S6 and S7 and Note S5, Supporting Information). The peak voltage generated with 1 GΩ of load resistance reached 45 mV, and the peak short-circuit current reached 100 pA for 0.39% strain and 40 mm s^{-1} strain rate. The maximum instantaneous power reached 2.54 pW at a load resistance of 500 MΩ (Figure S8, Supporting Information), and the conversion efficiency of the flexible m-WSe_2-based PEH reached 2.41% and sustained for over 1000 cycles (Figures S9–S11, Notes S6 and S7, and Table S1, Supporting Information). There were no electrical outputs from the bare PET substrate without an m-WSe_2 (Figure S12, Supporting Information).

We investigated the piezoresponse of the bilayer WSe_2 (b-WSe_2) by preparing two types of b-WSe_2. The first type consists of b-WSe_2 directly grown on a sapphire substrate via CVD (db-WSe_2), and the second consists of m-WSe_2 made via CVD and subsequently transferred onto another m-WSe_2, resulting in bilayer WSe_2 (tb-WSe_2). Previous reports have shown that the most common (2H) form (Bernal stacking) of b-WSe_2 loses its piezoelectricity due to the centrosymmetric structure, contrary to that of m-WSe_2, because the polarity is completely cancelled in the stacking mode, namely AA′ (**Figure 2**a).[1–3,6,19,23,25] In addition to the AA′ stacking mode, four stacking modes including AA, AB, AB′, and A′B are also allowed for db-WSe_2.[22,26] Depending on the relative stability of the different stacking modes, db-WSe_2 may have a mixed state of the different staking modes. Then the relative stability of the different stacking structures determines the fractions of each stacking structure in the mixed state, which in turn influences the piezoelectricity of the bilayers. Therefore, DFT calculations were performed to examine the relative stability of the db-WSe_2 with the five stacking modes. Three stacking structures, AA′, AB, and AB′, have relatively low energies compared to the A′B and AA stacking structures, and their difference in energy is

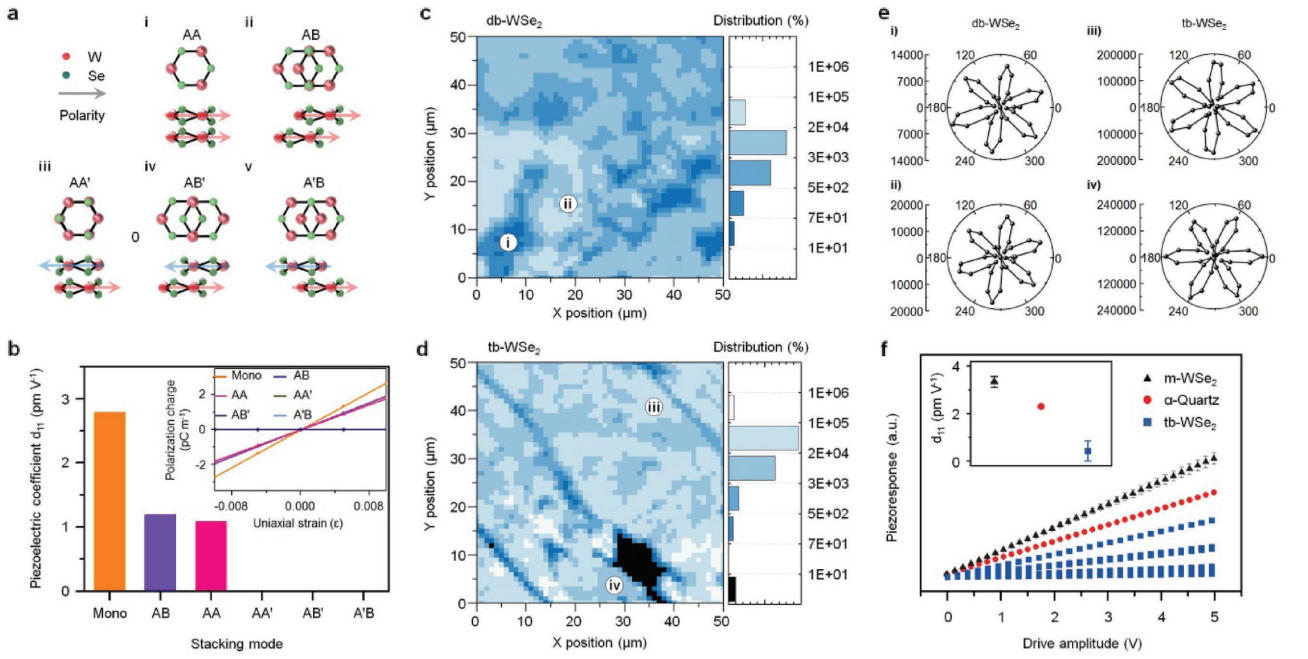

Figure 2. a) Stacking structure for bilayer-WSe_2. AA and AB stacking exhibit polarity in the same direction while AA′, AB′, and A′B exhibit polarity in the opposite direction. b) Simulated piezoelectric coefficient (d_{11}) of monolayer WSe_2 (2.79 pm V^{-1}), AA stacked WSe_2 (1.08 pm V^{-1}), and AB stacked WSe_2 (1.19 pm V^{-1}). Inset: piezoelectric characteristics of the monolayer and bilayer WSe_2 with different stacking orders (AA, AB, AA′ AB′, and A′B), using a density functional theory simulation. The SHG intensity mapping images of c) db-WSe_2 and d) tb-WSe_2. e) Polar plots of the SH intensity from db-WSe_2 and tb-WSe_2 as a function of the crystal's azimuthal angle θ. f) Lateral PFM result for m-WSe_2 (black triangle), tb-WSe_2 (blue square), and α-quartz (red circle). Inset: measured lateral piezoelectric coefficient (d_{11}) of m-WSe_2 (3.26 ± 0.3 pm V^{-1}), tb-WSe_2 (0–1.5 pm V^{-1}), and α-quartz (2.3 pm V^{-1}).

not significant (Figure S13 and Note S8, Supporting Information). The AA′ stacking structure is the most stable, which is consistent with the WSe_2 bilayer with Bernal stacking. The difference in energy for the three, AA′, AB, and AB′, is not significant, indicating that the fractions of AB and AB′ stacking structures are not negligible, but the AB′ stacking structure does not have piezoelectricity (see the piezoelectric coefficient calculation below). Therefore, a low piezoelectricity would be expected in the db-WSe_2. However, the tb-WSe_2 fabricated using the transfer method is expected to show an increase in its piezoelectricity due to the increase in degrees of freedom in the bilayer symmetry. Since the transfer method alleviates the restriction of a geometric relationship between the two layers, various stacking structures are available in the b-WSe_2, leading to an improvement in noncentrosymmetry in the bilayers. The piezoelectric coefficients e_{ijk} of the five stacking structures were also calculated via first-principles using Equations (1)

$$e_{ijk} = \left(\frac{\partial P_i}{\partial \varepsilon_{jk}}\right)_{E,T} = -\left(\frac{\partial \sigma_{jk}}{\partial E_i}\right)_{\varepsilon,T} \quad (1)$$

where P is the polarization, σ is the stress, ε is the strain, and E is the electric field. Although the piezoelectric coefficients e_{ijk} are more appropriate to evaluate the energy harvesting efficiency, the piezoelectric coefficients e_{ijk} are not available from the experiments. Therefore, subsequent calculations were made for the elastic modulus matrices, allowing for the further calculation of the piezoelectric coefficients d_{ijk} (Note S9, Supporting Information) as well as a comparison with the experimental values. The symmetry analysis of the stacking structures and the calculation of the elastic modulus tensor within the point group were performed to convert the piezoelectric coefficients from e_{ijk} to d_{ijk}. The piezoelectric coefficients e_{11} calculated for b-WSe_2 with various stacking configurations are shown in Figure 2b (Inset). As expected from the symmetry, no piezoelectricity is obtained in the AA′, AB′, and A′B stacking configurations, but piezoelectricity is obtained in the AA and AB stacking configurations that have the same polarization directions in each layer. Furthermore, the AA and AB stacked b-WSe_2 retain a large piezoresponse e_{11}, i.e., 1.79×10^{-10} and 1.93×10^{-10} C m^{-1}, respectively, that is comparable to that of m-WSe_2 (2.69×10^{-10} C m^{-1}). The piezoelectric coefficients d_{11} of the AA and AB stacked b-WSe_2 were also large, i.e., 1.08 and 1.19 pm V^{-1}, respectively, when compared to that of m-WSe_2 (d_{11} = 2.79 pm V^{-1}), as shown in Figure 2b. The d_{11} of m-WSe_2 is in reasonable agreement with the experimental value of 3.26 ± 0.3 pm V^{-1}. A summary of the simulation results are shown in **Table 1**. Therefore, the theoretical calculation of the energy and piezoresponse with several stacking configurations suggests an improvement in the piezoelectricity of tb-WSe_2, compared to that in db-WSe_2. To confirm the improvement in the piezoelectricity of tb-WSe_2, we first identified the orientation of db-WSe_2 and tb-WSe_2 by conducting SHG measurements. Figure 2c,d shows mapping images of the SHG intensity measured for the db-WSe_2 and tb-WSe_2 by observing a frequency-doubled reflectance signal over the area. While a weak signal at λ_{sh} was detected from the db-WSe_2, as expected for the Bernal stacking structure, the signal became relatively strong for the tb-WSe_2 corresponding to turbostratic stacking structure. However, the

Table 1. Summary of DFT simulation results.

Stacking mode	Point group	C_{11} [N m^{-1}]	C_{12} [N m^{-1}]	Young's modulus [N m^{-1}]	e_{11} [10^{-10} C m^{-1}]	d_{11} [pm V^{-1}]
Monolayer	D_{3h} ($\bar{6}m2$)	119.30	22.93	114.89	2.69	2.79
AA stacking	D_{3h} ($\bar{6}m2$)	206.45	41.36	198.16	1.79	1.08
AB stacking	C_{3v} ($3m$)	204.03	42.35	195.24	1.93	1.19
AA′ stacking	D_{3d} ($\bar{3}m$)	205.93	42.12	197.31	0	0
AB′ stacking	D_{3d} ($\bar{3}m$)	202.79	41.94	194.12	0	0
A′B stacking	D_{3d} ($\bar{3}m$)	206.37	41.24	198.13	0	0

intensity of the SHG signal in a small area of tb-WSe_2 was also very weak, as is expected for the centrosymmetry stacking order resulting from random stacking by the transfer method. The polar plots of the SH intensity from db-WSe_2 and tb-WSe_2 as a function of the crystal's azimuthal angle θ shows clear six-fold symmetry (Figure 2e). Moreover, the direct piezoelectric coefficient in the tb-WSe_2 was obtained by measuring the piezoresponse of the tb-WSe_2 using lateral PFM measurements. Figure 2f shows the piezoresponse of the m-WSe_2, α-quartz, and tb-WSe_2, and the piezoelectric coefficient d_{11} of the tb-WSe_2 was calculated based on its slope into 0–1.5 pm V^{-1}. Due to the random turbostratic stacking of the tb-WSe_2 layers, a part of the tb-WSe_2 are expected to have a centrosymmetric crystal that cancels the piezoelectricity (AA′, AB′, and A′B stacking) while other part of the tb-WSe_2 still maintains the piezoelectricity (AA and AB stacking) due to the increase in degrees of freedom of the bilayer symmetry, which is in reasonable agreement with the DFT simulation and SHG results. The db-WSe_2 does not show any piezoresponse (Figure S14, Supporting Information).

Bilayer TMD materials are known to have outstanding mechanical properties when compared to monolayer TMD materials due to the high Young's modulus and interlayer sliding effect of the bilayer TMD materials (Figure S15 and Note S10, Supporting Information).[11,12] Accordingly, tb-WSe_2 is expected to show a high mechanical durability compared to m-WSe_2, which is a very important factor in piezoelectric

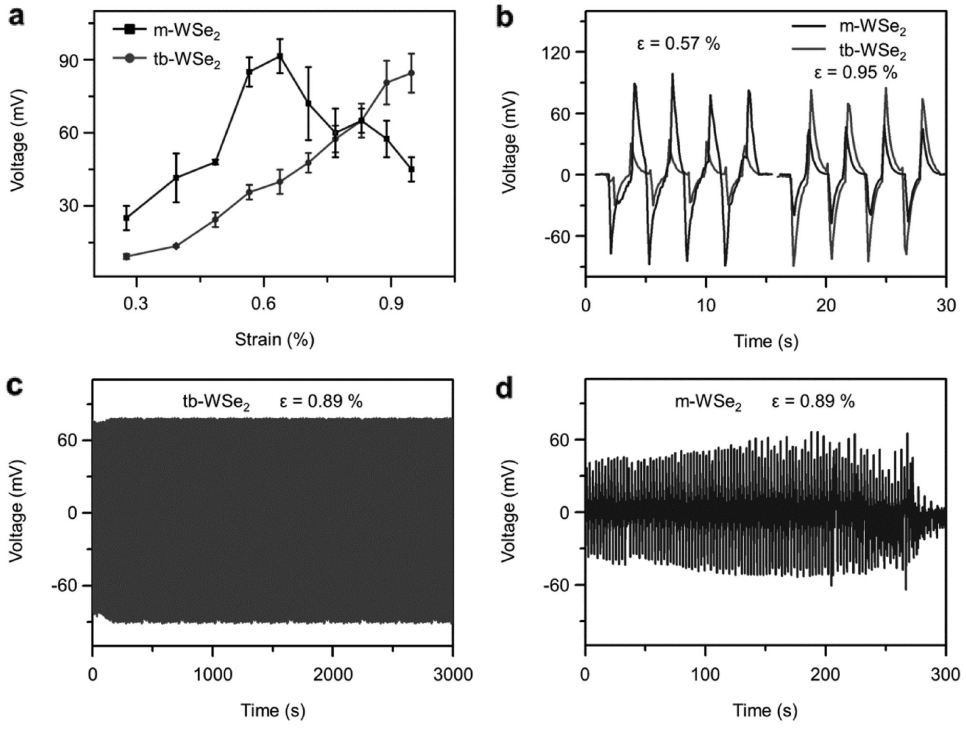

Figure 3. Investigation of the mechanical stability in mono/bi-layers WSe_2. a) Piezoelectric peak output voltages of m-WSe_2 and tb-WSe_2 as a function of strain with 1 GΩ of load resistance. b) Piezoelectric output voltage of m-WSe_2 (black line) and tb-WSe_2 (red line) with a low strain (0.57%) and high strain (0.95%). c,d) The durability test results conducted to compare the mechanical stability of the tb-WSe_2 and m-WSe_2 based PEHs with 0.89% of strain for more than 1000 cycles.

energy harvesting applications. The mechanical durability of m-WSe_2 and tb-WSe_2 based PEH is investigated by measuring the output performance of m-WSe_2 and tb-WSe_2 based PEHs as a function of the strain (**Figure 3**a,b and Figure S16, Supporting Information). The m-WSe_2 is expected to generate a higher output power than the tb-WSe_2 as a result of the higher piezoelectric coefficient d_{11} of the m-WSe_2. The peak output voltages generated for the m-WSe_2 increase linearly up to about 90 mV at 0.64% of strain and are dramatically reduced after 0.64% of strain as a result of a fracture in the m-WSe_2 (Figure 3a, and Figure S17, Supporting Information). On the other hand, the tb-WSe_2 exhibits a linear increase in output voltage of up to 0.95% of strain, reaching 85 mV and resulting in a high elasticity in the tb-WSe_2. The maximum instantaneous power was 4.05 pW with tb-WSe_2 at 0.89% of strain, and it was stable for over 1000 cycles (Figure 3c, Figure S18a and Table S2, Supporting Information). On the other hand, a maximum power of only 2.05 pW could be achieved with m-WSe_2 at a strain of 0.89%, and the power decreased significantly with repeated strain (Figure 3d and Figure S18b, Supporting Information). Therefore, the high piezoelectric performance and outstanding mechanical durability observed for tb-WSe_2 suggests that the proposed transfer method is the proper approach to obtain reliable WSe_2-based PEHs.

We have now demonstrated that the tb-WSe_2 sample exhibits reliable piezoelectricity with high power. However, the output power should still be further enhanced to allow for practical applications. PEHs can be integrated in a package to improve output power using a multi electrode patterning design on large-area tb-WSe_2 (**Figure 4**a). We fabricated five integrated PEHs in a single substrate and confirmed the direction of the piezoelectric polarity by examining each component of the piezoelectric output (Figure 4b,c, Figure S19, and Note S11, Supporting Information). The 14 working PEHs were successfully integrated among the 20 PEHs, and the measured output current linearly increased up to 1.4 nA as the number of parallel connections increased (Figure 4d). The output voltages of the parallel connected PEHs show an almost similar output voltage for the single PEHs (Figure 4e and Figure S20, Supporting Information). A very small, commercially available LCD was used for the test. The number "1" was selected as the output for the LCD screen, and the LCD was directly connected

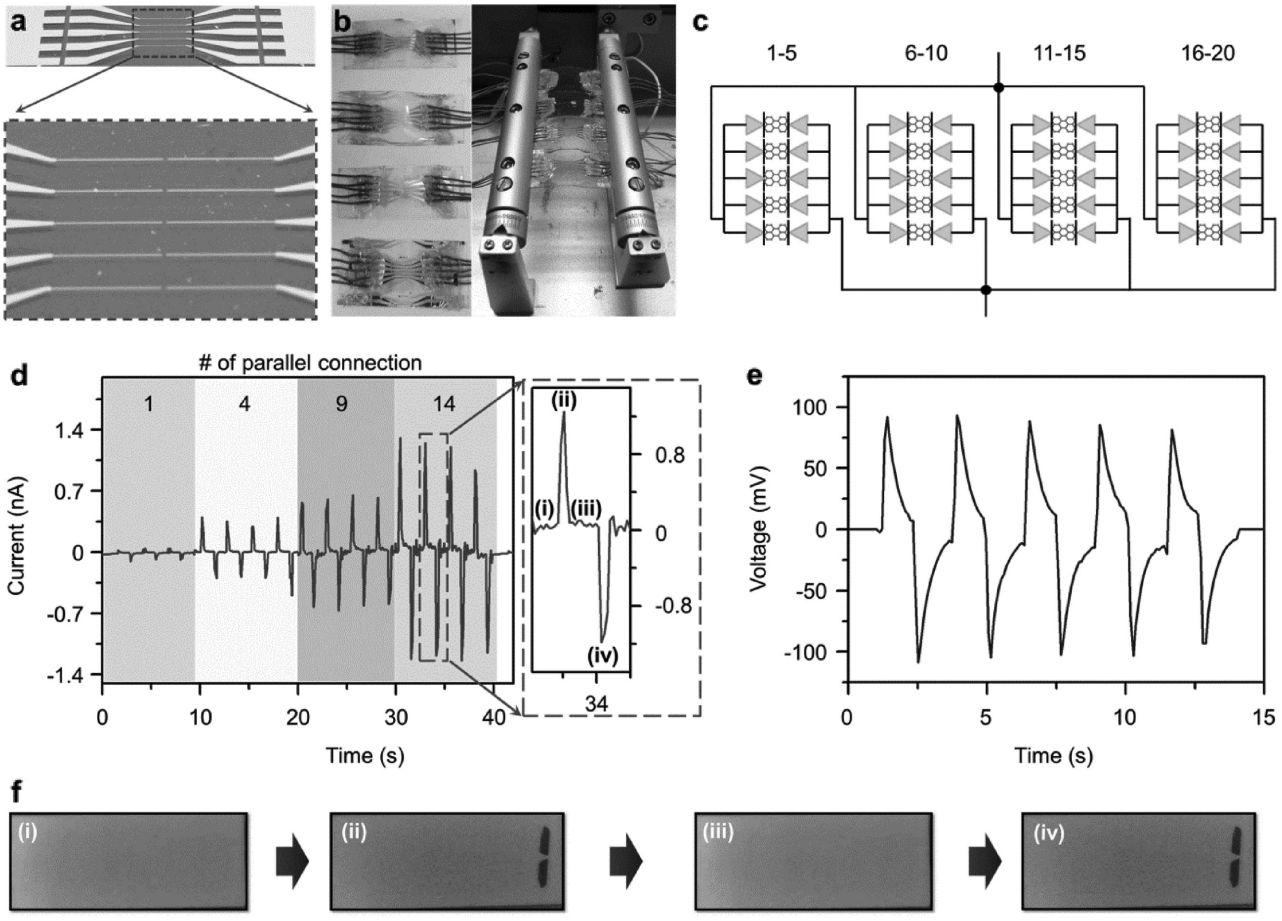

Figure 4. Demonstration of self-powered LCD operated by the integrated large-area tb-WSe_2 based PEHs. a) Image of an array consisting of five tb-WSe_2 PEH. b) Cu wire connected 20 tb-WSe_2 based PEHs (left) and PEHs on the bending machine (right). c) Schematic of the parallel connection of the 20 PEHs to improve the output current. d) Measured output currents for the integrated tb-WSe_2 PEHs as a function of the number of parallel connections. The right-hand part of (d) is an enlarged single cycle of the piezoelectric output. e) Measured output voltages of the integrated tb-WSe_2 PEHs with 1 GΩ of load resistance. f) Four snapshots taken from a full cycle driving of an LCD by the 14 integrated monolayer WSe_2 PEHs.

to the PEHs. Figure 4f shows a series of snapshots taken from the LCD when the PEHs were bent and released with 0.95% of strain and 40 mm s^{-1} of strain rate, showing a blinking number "1" that corresponded to the piezoelectric signal. This is the first demonstration of a 2D WSe_2-based PEH for self-powered electronics, indicating the need for further research for sensors, actuators, and energy harvesting applications.

In conclusion, we have demonstrated the piezoelectricity in large-area m-WSe_2 and tb-WSe_2 grown via CVD. The piezoelectric coefficient of the m-WSe_2 and the tb-WSe_2 measured using the lateral PFM method was as much as 3.26 pm V^{-1} and 1.5 pm V^{-1}, respectively. Moreover, reliable piezoelectricity in the tb-WSe_2 was also investigated by conducting a simulation and an experiment. The tb-WSe_2 exhibits good mechanical stability at a strain of up to 0.95%, and it generated an output voltage of 85 mV. The high output power, flexibility, and mechanical reliability over a wide range of strain of the tb-WSe_2 based PEH demonstrates its potential for use in mechanical sensors, actuators and energy sources for wearable and body-implantable electronics. In addition, our approach can be applied to other 2D TMD piezoelectric materials.

Experimental Section

Fabrication of Samples: Monolayer large-area WSe_2 was synthesized on a sapphire substrate via CVD with Se (0.2 g, 99.99%) and WO_3 (0.01 g, 99.995%) powders. Argon gas was used as a carrier gas, and hydrogen gas served as the reductant, with a flow rate of 190 and 10 sccm, respectively. The pressure in the chamber was higher than 50 Torr, and the synthesized monolayer WSe_2 was transferred to the appropriate substrate with a simple wet transfer method. The sample fabrication details are available in Note S1 (Supporting Information).

Raman Spectrum Measurements: The number of WSe_2 layers was confirmed via Raman spectroscopy. The Raman spectra were collected using a micro-Raman spectrometer system (WITec, Alpha300 M) with a 532 nm laser and a 100× (0.9 NA) objective lens. The grating for the measurement was of 1800 g mm^{-1}.

Lateral PFM Measurements: AFM-based investigations were carried out using an AFM (Park Systems, XE-100), and the piezoelectric property of the monolayer WSe_2 samples was confirmed using a PFM equipped with nonconductive silicon tips (spring constant of 3 N m^{-1}) (Budget Sensors, Multi 75-G), operating in the contact mode to image the topography and relative polarization via PFM. A lock-in amplifier (Stanford Research SR830) was also used to detect the piezoresponse signal.

Electrical Output Characterizations: An electrometer (Keithley 6514) with 200 TΩ input impedance was used to measure the voltage signals from the device, and a Keithley 6485 Picoammeter was used to measure the low-noise current in order to detect currents generated by the WSe_2-based piezoelectric devices. A bending machine made by Z-Tech (Korea) was used to apply the programmed driving strain inputs.

DFT Simulations: All calculations were conducted using density functional theory (DFT) implemented within the Vienna Ab initio Simulation Package.[27,28] The generalized gradient approximation with Perdew–Burke–Ernzerhof parameterization[29] was used to treat the exchange-correlation effect. The projector augmented wave method with a cutoff energy of 800 eV for the plane wave basis set was used.[30] To consider the van der Waals interaction between two layers, we used the DFT-D2 method of Grimme.[31] The Brillouin zone was sampled with a gamma-centered 14 × 14 × 1 k meshes. A slab supercell (total length of 40 Å) for monolayer or bilayer WSe_2 consists of the WSe_2 layer and a vacuum region separating the WSe_2 layers to prevent the interaction between the periodic images. All atoms in the supercell were fully relaxed until Hellman–Feynman forces on each atom were less than 0.001 eV $Å^{-1}$.

SHG Measurement: The SHG experiments were performed by using a Ti-sapphire femtosecond laser (Coherent Vitarat-T). The wavelength of the source was 800 nm, and the pulse width was about 100 fs with a repetition rate of 80 MHz. The fundamental wave pulse had 5 mW of average power, and it was focused on the sample to a diameter of about 1 μm by using a 50× objective lens (0.75 NA). Short-pass and band-pass filters were employed to isolate the second harmonic light, and its intensity was detected with a photomultiplier tube.

Supporting Information

Supporting Information is available from the Wiley Online Library or from the author.

Acknowledgements

J.-H.L., J.Y.P., and E.B.C. contributed equally to this work. This work was financially supported by a grant from Basic Science Research Program (2015R1A2A1A05001851) through the National Research Foundation (NRF) of Korea Grant funded by the Ministry of Science, ICT & Future Planning and a grant from the Center for Advanced Soft Electronics (CASE) under the Global Frontier Research Program (NRF–2013M3A6A5073177). Computational resources for DFT simulation were supported by KISTI supercomputing center (KSC-2015-C3-0012).

Conflict of Interest

The authors declare no conflict of interest.

Keywords

2D materials, atomic stacking, nanogenerators, piezoelectricity, tungsten diselenide

Received: December 9, 2016
Revised: April 7, 2017
Published online:

[1] W. Wu, L. Wang, Y. Li, F. Zhang, L. Lin, S. Niu, D. Chenet, X. Zhang, Y. Hao, T. F. Heinz, J. Hone, Z. L. Wang, *Nature* **2014**, *514*, 470.
[2] H. Zhu, Y. Wang, J. Xiao, M. Liu, S. Xiong, Z. J. Wong, Z. Ye, Y. Ye, X. Yin, X. Zhang, *Nat. Nanotechnol.* **2015**, *10*, 151.
[3] K.-A. N. Duerloo, M. T. Ong, E. J. Reed, *J. Phys. Chem. Lett.* **2012**, *3*, 2871.
[4] K. H. Michel, B. Verberck, *Phys. Rev. B* **2009**, *80*, 224301.
[5] M. T. Ong, E. J. Reed, *ACS Nano* **2012**, *6*, 1387.
[6] Y. Li, Y. Rao, K. F. Mak, Y. You, S. Wang, C. R. Dean, T. F. Heinz, *Nano Lett.* **2013**, *13*, 3329.
[7] X. Liu, X. Yang, G. Gao, Z. Yang, H. Liu, Q. Li, Z. Lou, G. Shen, L. Liao, C. Pan, Z. L. Wang, *ACS Nano* **2016**, *10*, 7451.
[8] W. Liu, Y. Zhou, A. Zhang, Y. Zhang, Z. L. Wang, *Appl. Phys. Lett.* **2016**, *108*, 181603.
[9] Y. Zhou, X. Huang, A. Zhang, Y. Zhang, Z. L. Wang, *Nano Res.* **2016**, *9*, 800.
[10] K.-A. N. Duerloo, E. J. Reed, *Nano Lett.* **2013**, *13*, 1681.
[11] S. Bertolazzi, J. Brivio, A. Kis, *ACS Nano* **2011**, *5*, 9703.

[12] K. Liu, Q. Yan, M. Chen, W. Fan, Y. Sun, J. Suh, D. Fu, S. Lee, J. Zhou, S. Tongay, J. Ji, J. B. Neaton, J. Wu, *Nano Lett.* **2014**, *14*, 5097.
[13] J.-K. Huang, J. Pu, C.-L. Hsu, M.-H. Chiu, Z.-Y. Juang, Y.-H. Chang, W.-H. Chang, Y. Iwasa, T. Takenobu, L.-J. Li, *ACS Nano* **2014**, *8*, 923.
[14] J. Chen, B. Liu, Y. Liu, W. Tang, C. T. Nai, L. Li, J. Zheng, L. Gao, Y. Zheng, H. S. Shin, H. Y. Jeong, K. P. Loh, *Adv. Mater.* **2015**, *27*, 6722.
[15] M.-H. Chiu, C. Zhang, H.-W. Shiu, C.-P. Chuu, C.-H. Chen, C.-Y. S. Chang, C.-H. Chen, M.-Y. Chou, C.-K. Shih, L.-J. Li, *Nat. Commun.* **2015**, *6*, 7666.
[16] W. Zhao, Z. Ghorannevis, K. K. Amara, J. R. Pang, M. Toh, X. Zhang, C. Kloc, P. H. Tan, G. Eda, *Nanoscale* **2013**, *5*, 9677.
[17] C. Huang, S. Wu, A. M. Sanchez, J. J. P. Peters, R. Beanland, J. S. Ross, P. Rivera, W. Yao, D. H. Cobden, X. Xu, *Nat. Mater.* **2014**, *13*, 1096.
[18] K. L. Seyler, J. R. Schaibley, P. Gong, P. Rivera, A. M. Jones, S. Wu, J. Yan, D. G. Mandrus, W. Yao, X. Xu, *Nat. Nanotechnol.* **2015**, *10*, 407.
[19] H. Yu, D. Talukdar, W. Xu, J. B. Khurgin, Q. Xiong, *Nano Lett.* **2015**, *15*, 5653.
[20] G. Wang, X. Marie, I. Gerber, T. Amand, D. Lagarde, L. Bouet, M. Vidal, A. Balocchi, B. Urbaszek, *Phys. Rev. Lett.* **2015**, *114*, 097403.
[21] M.-Y. Li, Y. Shi, C.-C. Cheng, L.-S. Lu, Y.-C. Lin, H.-L. Tang, M.-L. Tsai, C.-W. Chu, K.-H. Wei, J.-H. He, W.-H. Chang, K. Suenaga, L.-J. Li, *Science* **2015**, *349*, 524.
[22] W. T. Hsu, Z.-A. Zhao, L.-J. Li, C.-H. Chen, M.-H. Chiu, P.-S. Chang, Y.-C. Chou, W.-H. Chang, *ACS Nano* **2014**, *8*, 2951.
[23] S. K. Kim, R. Bhatia, T.-H. Kim, D. Seol, J. H. Kim, H. Kim, W. Seung, Y. Kim, Y. H. Lee, S.-W. Kim, *Nano Energy* **2016**, *22*, 483.
[24] R. Bechmann, *Phys. Rev.* **1958**, *110*, 1060.
[25] K. H. Michel, B. Verberck, *Phys. Rev. B* **2011**, *83*, 115328.
[26] A. A. Puretzky, L. Liang, X. Li, K. Xiao, B. G. Sumpter, V. Meunier, D. B. Geohegan, *ACS Nano* **2016**, *10*, 2736.
[27] G. Kresse, J. Hafner, *Phys. Rev. B* **1994**, *49*, 251.
[28] G. Kresse, J. Furthüller, *Phys. Rev. B* **1996**, *54*, 169.
[29] J. P. Perdew, K. Burke, M. Ernzerhof, *Phys. Rev. Lett.* **1996**, *77*, 3865.
[30] P. E. Blöchl, *Phys. Rev. B* **1994**, *50*, 17953.
[31] S. Grimme, *J. Comput. Chem.* **2006**, *27*, 1787.